# The giant *Staphylococcus epidermidis* surface protein Embp binds selectively to fibrillated fibronectin through a Velcro-like mechanism

Nasar Khan[1†], Hüsnü Aslan[1†‡], Henning Büttner[2], Holger Rohde[2], Thaddeus Wayne Golbek[3], Steven Joop Roeters[3,4], Sander Woutersen[4], Tobias Weidner[3], and Rikke Louise Meyer[1,5*]

1: Interdisciplinary Nanoscience Center (iNANO), Aarhus University, 8000 Aarhus, Denmark.
2: Institute for Medical Microbiology, Virology and Hygiene, University Medical Centre Hamburg-Eppendorf, 20246 Hamburg, Germany.
3: Department of Chemistry, Aarhus University, 8000 Aarhus C, Denmark.
4: Van 't Hoff Institute of Molecular Sciences, University of Amsterdam, 1098XH, Amsterdam, the Netherlands.
5: Department of Biology, Aarhus University, 8000 Aarhus C, Denmark.
† These authors contributed equally to this work.
‡ Current affiliation: DFM – Danish National Metrology Institute, Kogle Alle 5, 2970 Hoersholm, Denmark
* Corresponding author: rikke.meyer@inano.au.dk

## Abstract

*Staphylococcus epidermidis* is a major cause of implant-associated infections. It attaches to implants via adsorbed host proteins, and one prominent adhesin is the fibronectin-binding protein Embp. This study aims to determine how *S. epidermidis* can attach to surfaces via adsorbed fibronectin, when fibronectin is also abundant in solution. We hypothesize that Embp interacts selectively with adsorbed fibronectin if adsorption introduces a conformational change. We produced a model system in which Fn adsorbed in either globular or fibrillated conformation. Embp-mediated attachment occurred exclusively to fibrillated Fn, and involved subdomain F3 12$^{th}$-14$^{th}$, which is buried in globular Fn. Single-molecule force spectroscopy revealed a Velcro-like interaction, as a single of the 60 Fn-binding repeats interacted weakly, while 15 FG-repeats attached strongly with the fibrillated ligand. This mechanism enables selective and strong attachment to immobilized Fn via a single surface protein: a mechanism that proved particularly beneficial for attachment under high flow conditions.

## INTRODUCTION

Biomedical implants, such as catheters, prosthetics, vascular grafts, and similar devices have revolutionized the medical field. However, implants can lead to severe infections (*1*). Staphylococci,

particularly *Staphylococcus aureus* and *Staphylococcus epidermidis* are the culprits of many implant-associated infections (*2*). Despite is low virulence, *S. epidermidis* thrives in implant-associated infections due to its prowess in biofilm formation. Bacteria in the biofilm evade phagocytosis by immune cells (*3*), and the immune system can therefore not eradicate the infections. Furthermore, a fraction of the cells enter a dormant state in which they are highly tolerant to antibiotics (*4*). With the rise in use of biomedical implants, there is an urgent and growing need to understand how biofilm infections arise, such that new strategies for preventative treatment can be developed.

*S. epidermidis* attaches to implant surfaces via adsorbed extracellular matrix (ECM) components (*5, 6*). *S. epidermidis* expresses an array of surface-bound proteins that bind to human ECM proteins, such as fibrin, fibronectin, vitronectin, and collagen to initiate biofilm formation(*7*). One of these is the extracellular matrix binding protein (Embp), which is found in 90% of clinical isolates of *S. epidermidis* (*8, 9*), suggesting that this giant 1 MDa protein is important for the pathogenicity of *S. epidermidis.* Embp contains a number of repetitive domains. These were originally described based on sequence similarity to be 21 “Found in Various Architecture” (FIVAR) repeats and 38 alternating repeats of “G related Albumin Binding” (GA) motif and FIVAR repeats combined, named FIVAR-GA repeats. After the crystal structure was recently solved, the domain structure was updated and consists of 10 170-aa F-repeats that each represent two FIVAR modules, and 40 125-aa FG-repeats that each represent the previously termed FIVAR-GA module (*10*). Embp binds to fibronectin (Fn), and it is presumed that this interaction aids the colonization of the host (*11*).

Fn deposition can occur around implants (*12*) and may offer a site for bacterial attachment. We wondered how bacteria like *S. epidermidis* can colonize implant surfaces by interacting with adsorbed Fn when the same protein is abundant in the blood in a soluble form. Presumably, Fn-binding proteins on the bacterial cell surface become occupied with soluble Fn before being able to interact with Fn on the implant surface. The aim of this study was determine how pathogens overcome this dilemma and bind to host ECM proteins on tissue or implant surfaces while ignoring soluble forms of the same protein. Understanding how pathogens selectively colonize implant surfaces reveals conceptual mechanisms for how pathogens control their location and fate in the host.

In this study, we investigate Embp’s interaction with Fn. Fn circulates in bodily fluids in a compact globular form (*13*), while fibrillated Fn contributes to the formation of ECM assembly (*14*). It is the stretching of Fn upon interacting with integrin that results in exposure of self-binding domains used in fibrillation, and this mechanism ensures that Fn only fibrillates in the extracellular matrix of tissue and not in the blood stream (*15*). We hypothesize that *S. epidermidis* interacts selectively with

the fibrillated conformation of Fn, and that the fibrillated ligand provides an opportunity for a strong multi-valent interaction via the many repetitive binding sites of Embp. We used a model system of polymer-coated surfaces that facilitates Fn adsorption in globular vs fibrillated conformation, and subsequently probed Embp's interaction with Fn, leading to bacterial attachment. Using native and recombinant Embp proteins in a series of analyses at the population-, single-cell-, and single-molecule levels, we confirmed that Embp selectively interacts with fibrillated Fn. The interaction is a Velcro-like mechanism where multiple binding-domains must interact simultaneously to facilitate cell attachment. Being able to attach with strong adhesion force via a single protein is particularly beneficial for *S. epidermidis* if attachment under high sheer stress, such as in the vascular system, and it was exactly under these conditions that Embp gave the cells and advantage. Our findings can further the current understanding of bacterial attachment and help in developing possible solutions to combat implant-associated infections.

## RESULTS

### Embp does not interact with soluble Fn

We hypothesized that Embp selectively binds to fibrillated Fn, which would allow the bacteria to colonize tissue without its Fn-binding adhesins being blocked by soluble Fn in the bloodstream. To study the interaction between Embp and Fn, we expressed Embp fusion proteins comprised of either 5 F-repeats (Embp_5F) or 9 FG-repeats (Embp_9FG), each fused to the native export signal and anticipated C-terminal cell wall anchor region (*10*), in the surrogate host *Staphylococcus carnosus* TM300, which has no other mechanisms for attachment to Fn. The full-length Embp is too large to clone into a surrogate host, and it was therefore not possible to investigate the full-length Embp protein. However, expression of the two different Embp fragments allowed us to study their interactions individually. The presence of either of these fragments on the cell surface was confirmed by immunofluorescence staining (Figure S1).

Exposure to fluorescently conjugated Fn showed that neither F- nor FG-repeats facilitated adsorption of soluble Fn to the cell surface (Figure S2). As expected, *S. epidermidis* expressing native Embp did not bind soluble Fn on the cell surface either either (Figure S2), concluding that Embp does not interact with Fn in its soluble, globular conformation.

### Embp interacts exclusively with adsorbed Fn in fibrillar conformation

In order to further investigate Embp's interaction with Fn in different conformations, we produced a model system in which Fn was adsorbed to a surface in either the globular of fibrillated conformation. Previous research had shown that Fn fibrillates when adsorbed on surfaces coated with poly (ethyl acrylate) (PEA), while it remains globular on poly (methyl acrylate) (PMA) (*16-18*). The two polymer coatings have similar physico-chemical properties, but the ethyl side group of PEA provides sufficient mobility of the adsorbed protein to facilitate fibrillation (*19, 20*). The presence of polymer coatings was confirmed by atomic force microscopy (AFM) (Figure S3), and imaging of adsorbed Fn confirmed the two different conformations (Figure 1A, C). Fn spontaneously organized into a fibrillated network on PEA while fibrillated structures did not form on PMA. This structural assignment was corroborated by Fourier-transform infrared (FTIR) spectra, in which the peak positions indicate that Fn adsorbed to PMA adopts a mostly antiparallel β-sheet type secondary structure (*21*), similar to the globular, solution-state spectrum, while Fn on PEA adopts an extended parallel β-sheet type structure (Figure S6).

In order to ascribe any differences in adhesion to the difference in the conformation of Fn and not the amount of adsorbed Fn, we analysed the quantity of protein on the two surfaces. The FTIR analysis, as well as XPS analysis determined that the amount of adsorbed protein was similar on the two polymer surfaces (Figure 1B and D, Table S1). The XPS survey scan and high-resolution $C_{1s}$ XPS plots are shown in Figure S4 and Figure S5. Furthermore, FTIR spectroscopy also confirmed differences in the conformation of the adsorbed Fn, as peak frequencies indicate that the Fn adsorbed to PMA adopts a mostly antiparallel β-sheet type secondary structure, while the Fn on PEA appears to adopt an extended parallel β-sheet type structure (Figure S6).

Embp-mediated bacterial attachment to the two different conformations of Fn was then measured using a flow-cell system where the number of attached bacteria was counted by microscopy. Adsorbed Fn strongly stimulated attachment of *S. carnosus* expressing Embp_5F or Embp_9FG, but only on surfaces where Fn was fibrillated (Figure 2A). Fn consists of two nearly identical subunits linked by a pair of disulfide bonds at the C terminal (*22*). Each subunit consists of three domains; F1, F2, and F3 (*23*). The globular and compact conformation of Fn is sustained by intramolecular electrostatic interactions between F1 $1^{st}$-$5^{th}$, F3 $2^{nd}$-$3^{rd}$, and F3 $12^{th}$-$14^{th}$ repeat (*24, 25*). Binding sites in these regions remain buried in such compact conformation; however, upon fibrillation on a surface or tissue interface, these binding sites become exposed (*26*). Since Embp only binds to fibrillated Fn, we hypothesize that it interacts with epitopes that are buried in the globular conformation, but become exposed in the fibrillated conformation. Indeed, it was previously

reported that *S. epidermidis* binds near the C terminal of Fn (*27*), and studies on recombinant Fn verified the interaction between Embp and the 12$^{th}$ repeat of the F3 domain (*11*). This repeat may be one of several interaction points and has not been confirmed in full-length Fn adsorbed in its natural conformation. To test the interaction between the 12$^{th}$ repeat of the F3 domain and the Fn-binding F- and FG-repeats, we repeated cell adhesion analysis on Fn-coated PEA after blocking the C-terminal heparin-binding domain II (F3 12$^{th}$-14$^{th}$ repeat) with antibody sc-18827. Control-samples were blocked with antibody F0916 specific for the F3 5$^{th}$ repeat (Figure 2B). Blocking the F3 12$^{th}$-14$^{th}$ repeat decreased the adherence of *S. carnosus* by approximately 62 % for Embp_5F and 64 % for Embp_9FG (Figure 2B), supporting that Embp interacts with this subdomain. As the adherence was not completely abolished by blocking the Fn binding site, we cannot exclude the possibility that Embp interacts with other epitopes in Fn. However, the F3 12$^{th}$-14$^{th}$ repeat is of major significance.

**Attachment strength mediated by Embp**

After learning that Embp interacts exclusively with fibrillated Fn, we probed the strength of this interaction by single-cell atomic force spectroscopy. Single *S. carnosus* expressing Embp_5F or Embp_9FG were attached to colloidal AFM probes, approached to a Fn-coated PMA or PEA surface with controlled force, and then retracted to detect the force needed to detach the cell from the surface. As expected, the force-distance curves obtained from these experiments show that both of the Embp fragments binds to fibrillated but not to globular Fn. The average maximum adhesion force between *S. carnosus* and surfaces with fibrillated Fn was 1.19 ± 0.21 and 1.16 ± 0.18 nN, respectively, for *S. carnosus* expressing Embp_5F or Embp_9FG (Figure 3). In contrast, the corresponding adhesion force to surfaces with globular Fn was only 0.16 ± 0.09 nN and 0.12 ± 0.04 nN. The adhesion force and the shape of the force-distance curves reflect multiple binding events between the cell and the Fn-coated surface. The multiple binding events could either be due to multiple Embp fragments on the cell surface interacting with Fn, or multiple interactions between a single Embp fragment and Fn.

**Embp binds to fibrillated Fn in a Velcro-like manner**

Embp contains 60 Fn-binding repeats, and it must be costly for *S. epidermidis* to produce this enormous 1 MDa protein. How might *S. epidermidis* benefit from the many repetitive binding-domains? We hypothesize that multivalent interactions can occur if the ligand for this giant adhesin is fibrillated, resulting in presentation of multiple binding domains in close proximity. Such

multivalent binding would in this case work in a similar manner as Velcro, as many weak binding events result in strong attachment. Such a Velcro-effect could provide adhesion forces strong enough to attach *S. epidermidis* to Fn via a single Embp protein. To investigate this hypothesis, we expressed and purified recombinant protein fragments that contained 1, 4, and 15 repeats of FG- repeats, attached them to an AFM cantilever using 6His-NTA interaction, and quantified their interaction with Fn by single-molecule force spectroscopy. In agreement with previous experiments, the FG-repeat did not interact with the globular form of Fn (Figure 4). The interaction force of a single FG-repeat with fibrillated Fn was also insufficient to be detected. However, the interaction force of 15 FG-repeats was 432 ± 48 pN with fibrillated Fn (Figure 4), confirming the value of multi-domain interaction with the fibrillated ligand.

**Embp facilitates attachment under high flow**

We probed the interaction mechanism between Embp and Fn expressing fusion proteins that contained only a few of the F- or FG-repeats displayed on the surface of *S. carnosus* which has no other adhesive proteins. *S. epidermidis* has many other cell wall anchored adhesins, and the key to understanding Embp's role in *S. epidermidis*' pathogenicity lies in understanding the circumstances where Embp-producing *S. epidermidis* strains are at an advantage. If oriented perpendicular to the cell surface, Embp could potentially stretch several hundred μm from the cell surface. Indeed, the hydrodynamic radius of *S. epidermidis* over-expressing Embp (2.3 ±0.4 μm) was significantly larger than for *S. epidermidis* lacking Embp (1.3 ±0.2 μm) (two-tailed t-test, n=3, $P<0.001$). We speculated that Embp would be more effective than other adhesins when *S. epidermidis* is attaching to Fn at high sheer stress. We therefore compared attachment of the two strains at low flow (1 mL $min^{-1}$, 1.8 dyn $cm^{-2}$) and high flow (18 mL $min^{-1}$, 31.7 dyn $cm^{-2}$), representative of the shear stress in arteries. Expression of Embp had little effect on attachment to adsorbed Fn at low flow, but at high flow, attachment was only possible in the strain expressing Embp (Figure 5).

## DISCUSSION

In this study, we show that the giant cell-surface protein Embp exclusively binds to fibrillated Fn because the binding site located at F3 $12^{th}$ -$14^{th}$ repeat is not accessible in the globular, soluble form of Fn. This discovery has implications for our understanding of how *S. epidermidis* colonizes host tissue and biomedical implants. Colonization and biofilm formation is the only virulence factor of *S. epidermidis* pathogensis, and it is therefore imperative to cause invasive diseases (*28*). Implants are

hot-spots for biofilm formation because they offer a surface for attachment. The implant surface is immediately covered by host proteins when it is inserted into the body, and bacterial attachment is assumed to occur via specific receptor-ligand interactions between adhesins on the bacterial cell and host proteins adsorbed to the implant surface. The abundance of the same host proteins in solution poses a dilemma: How can bacterial adhesins mediate attachment to implant surfaces via adsorbed proteins, if the same proteins are readily available in solution? Based on previously published evidence (*10*, *11*), we hypothesized that adsorption-induced conformational changes can affect how accessible a host protein is as a ligand for bacterial attachment. In the case of Embp-mediated attachment to Fn, the conformational change that triggers fibrillation of Fn on the implant surface is decisive for its availability as a ligand for bacterial attachment.

The selective interaction with fibrillated Fn illustrates how biology has solved the need for interaction with a protein in one location (the extracellular matrix of host tissue) while ignoring the same protein in another location (the bloodstream). Our results also challenge the general assumption that host proteins adsorb to implant surfaces and thereby provide an opportunity for bacterial attachment. Motivated by this general assumption, much research has been devoted to developing materials or coatings that prevent protein adsorption and thereby avoid bacterial attachment. However, our work raises the question of whether bacterial attachment can be diminished by controlling the conformational changes of adsorbed proteins rather than avoiding protein adsorption altogether. Biomaterials' susceptibility to biofilm formation is not only a question of how the surface topography and chemistry affects the amount and type of proteins adsorbed, but also how these parameters affect conformational changes of the adsorbed proteins. Indeed, previous *in vitro* studies of how serum proteins affect attachment of staphylococci has produced conflicting results. Some studies report increased attachment (*11*, *29-31*), while others report the opposite (*32*, *33*). Perhaps these discrepancies are linked to how the underlying material affected the conformation of adsorbed serum proteins.

The large number of repetitive domains in Embp and its homologs in *S. aureus* (Ebh) and *Streptococcus defectivus* (Emb) is unusual, and we wondered how pathogens benefit from producing adhesins with this repetitive structure. One benefit could be that the adhesin protrudes from the cell surface, which makes it easier for the adhesin to connect with its ligand despite the overall electrostatic repulsion caused by the electric double layer. At present, no experimental evidence is available to directly demonstrate the Embp organization located on the bacterial cell wall. However, given the stretched overall architecture revealed by structural analysis of Embp (*10*), it appears

plausible to assume that the molecule´s length is similar to that of *S. aureus* similar and the total length for its homolog in *S. aureus*, Ebh. Ebh is a 1.1 MDa protein with 52 repetitive domains, and its length was predicted to be 320 nm (*34*). We show that the hydrodynamic radius of *S. epidermidis* over-expressing Embp was approximately 1 μm larger than *S. epidermidis* lacking Embp. It is thus likely that Embp extends well beyond the electric double layer.

Another advantage of having many repetitive binding domains is the possibility for multivalent interaction with Fn. Such multivalency is only possible if Fn is fibrillated and thereby presenting many copies of the binding domain in close proximity of each other. Indeed, we show by single-molecule force spectroscopy that a single binding FG-repeat interacts weekly to Fn, while the interaction force of 15 FG-repeats was 432 ± 48 pN. We therefore propose that the selective interaction with fibrillated Fn results in part from the exposure of an otherwise buried binding domain in the fibrillated protein, and in part from the availability of multiple binding repeats to allow a multivalent interaction with sufficient strength to mediate attachment.

The typical strength of receptor-ligand bonds is about 20-200 pN (*35*). Hence the interaction between 15 FG-repeats and Fn resulted in a very strong bond, and the interaction with full sized Embp is likely to be much stronger. The force required to detach Embp from fibrillated Fn will depend on whether all binding repeats detach at once, or whether detachment can occur from the serial unbinding of the repeats one by one. This is akin to detachment of Velcro: The attachment is very strong, but detachment can be obtained by the serial unbinding of individual interactions. The force-distance curves can provide information about how detachment occurs. On a close inspection, it is clear that initial retraction events are the strongest and provide the highest adhesion force, indicating that multiple bonds are broken at the same time (Figure 4B). But we can also see multiple following perturbations as evidence to serial rupture, unfolding or stretching events. This holds true for interactions with a single FG-repeat as well as 15 FG-repeats. In this case, the perturbations likely arise from the stretching and ruptures of surface bound fibronectin yielding an average adhesion force of 92 ± 27 pN, which is around the detection limit for this setup. Similar results were observed for 4 repeating units with average adhesion force of 68 ± 43 pN. On the surfaces with globular Fn, little to no interaction was observed with all 1, 4 and 15 repeating units although 15 repeating units undergo certain irregular interactions. An explanation for the observed irregularities could be simply the protein's self-occupation/entanglement as would often happen with long polymer chains. Additionally, as can be seen from Figure 1, the surface distribution of Fn can vary depending on the

local density. This may be an insignificant problem for the dynamics of cell populations, however, when it comes to assessing individual cell's behavior, the local density can affect the results.

In conclusion, the specific binding domain and repetitive structure of Embp provides an opportunity for *S. epidermidis* to interact selectively and strongly with fibrillated Fn, using a single adhesive protein. The open question is how this unique Velcro-like of interaction plays into the pathology of *S. epidermidis* and other pathogens with homologs of this protein. The genome of *S. epidermidis* is highly variable, and not all isolates possess the same repertoire of genes for host colonization and biofilm formation (*36*). Embp, however, is present in two thirds of *S. epidermidis* isolates from orthopedic device-related infections (*36*) and 90 % of isolates from blood stream infections (*9*), which indicates some importance for its pathogenicity. Strong attachment via a single protein could be particularly advantageous in locations where high shear forces make attachment difficult, such as in the blood stream. Biofilms generally do not form in blood vessels, unless there is an implant or a lesion on the endothelium. Infections like endocarditis often start with such a lesion (*37*), which makes the site susceptible to bacterial attachment. Fibrillated Fn forms on the surface of platelets in the early stages of wound healing (*38*), and perhaps the abundance of fibrillated Fn plays role in the elevated infection risk. We show that Embp is required for attachment of *S. epidermidis* under high flow (Figure 5), pointing to a role for Embp in attachment of *S. epidermidis* e.g. to cardiovascular grafts. Future research in animal models will determine Embp's role in host and implant colonization in the cardiovascular system.

## MATERIALS AND METHODS

### Bacterial strains

*S. epidermidis* 1585 WT is a clinical isolate obtained from Rohde lab in UKE, Hamburg. *S. epidermidis* 1585Pxyl/tet *embp* (Embp overexpressed), *S. epidermidis* Δ*embp*, *S. carnosus* TM300 x pEmbp_5F (expressing 5 F-repeats) and *S. carnosus* TM300 x pEmbp_9FG (expressing 9 FG-repeats) were generated previously in the Rhode lab (*10*).

### Immunofluorescence of Embp fusion protein

Expression of Embp fusion protein in a non-adhesive surrogate host was critical for studying the interaction of Embp without interfering interactions from other adhesive proteins on the surface of *S. epidermidis*. We therefore started out by confirming the presence of Embp fragments on the surface of the surrogate host. *S. carnosus* TM300 WT, and *S. carnosus* TM300 x pEmbp_5F were grown

overnight in brain heart infusion (BHI) broth with 10 μg $ml^{-1}$ chloramphenicol (Sigma-Aldrich, Germany). Expression of Embp fragments in the mutant strains was induced with 200 ng $ml^{-1}$ anhydrotetracycline (AHT) after diluting the culture 100 times in BHI. Cells were grown for 6 hours at 37°C in a shaking incubator with 180 rpm until the 600 nm optical density ($OD_{600}$) reached approximately 1. Cells were harvested by centrifugation (4000 × *g* or 10 minutes) and resuspended in phosphate buffered saline (PBS). A droplet of the resuspended cells was placed on a SuperFrost Ultra Plus slides (Invitrogen, USA) for 45 minutes to allow the bacteria to adsorb. After washing off unbound cells, the bacteria were fixed with 4% paraformaldehyde for 30 minutes at room temperature and washed twice with PBS. Samples were blocked with 5% goat serum (Invitrogen, USA) for 45 minutes, washed, incubated with anti-Embp2588 IgG antibodies (*39*) diluted 1:200 in blocking buffer at room temperature for 1 hour, washed three times, and then incubated with the secondary antibody (Anti-rabbit IgG conjugated with Alexa Fluor 635, Invitrogen, USA) diluted 1:300 in blocking buffer for 1 hour at room temperature. Cells were then washed three times and stained with 10 μM SYTO 9 (Invitrogen, USA) in PBS for 10 minutes, washed 3 times, and visualized by confocal laser scanning microscopy (CLSM) (LSM700, Zeiss, Germany) using 488 excitation for SYTO 9, and 639 nm excitation Alexa Fluor 635 conjugated antibody, and a 63x Plan-Apochromat N/A 1.4 objective.

**Interaction of Embp with soluble Fn**

We first investigated if *S. epidermidis* or a surrogate host expressing Embp fragments interacted with soluble Fn in its globular conformation. *S. aureus* 29213 WT (positive control for soluble Fn binding) *S. epidermidis* 1585 WT, *S. epidermidis* 1585△*embp* (Embp knockout), were grown in BHI without antibiotics. *S. epidermidis* 1585Pxyl/tet *embp* (Embp overexpressed) was grown in BHI with 5 μg $ml^{-1}$ erythromycin, *S. carnosus* TM300 x pEmbp_5F (5 F-repeats) and *S. carnosus* TM300 x pEmbp_9FG (9 FG-repeats) were grown in BHI with 10 μg $ml^{-1}$ chloramphenicol. Expression of Embp, F- and FG-repeats in the mutant strains was induced with 200 ng $ml^{-1}$ anhydrotetracycline (AHT) after diluting the culture 100 times in BHI. Cells were grown for 6 hours at 37°C in a shaking incubator with 180 rpm until reaching $OD_{600}$ of approximately 1. Cells were harvested by centrifugation (4000 g for 10 minutes) and resuspended in PBS. A droplet of the resuspended cells was immobilized on a SuperFrost Ultra Plus slides (Invitrogen, USA) for 45 minutes to allow the bacteria to adsorb. The unabsorbed cells were removed by washing with PBS, and the adsorbed cells were then blocked with 3% BSA for 45 minutes. Cells were then incubated with 100 μg $ml^{-1}$ Fn in PBS (Sigma-Aldrich, F0895) for 60 minutes at room temperature. The unbound Fn was removed by washing three times with PBS. The samples were then fixed with 4% paraformaldehyde for 30

minutes at room temperature. Immunolabeling was then performed as described above, Anti-Fn mouse IgG (Sigma-Aldrich) diluted 1:100 in blocking buffer and the secondary antibody (Anti-mouse IgG conjugated with Alexa 635, Goat IgG - Invitrogen) diluted 1:300 in blocking buffer. Cells were stained and prepared for imaging as described above.

**Preparation of polymer-coated surfaces**

Quantification of interaction forces between Embp and Fn in its globular or fibrillated form would require that Fn was immobilized to a surface. We used a previously published model system (*20, 40*) to generate Fn-coated surfaces that displayed Fn in these two conformations, while the physicochemical properties of the underlying surface was very similar, namely PEA and PMA. Polymers of ethyl acrylate and methyl acrylate were synthesized from their monomers (99% pure, Sigma-Aldrich, Germany) using radical polymerization. Benzoin (98% pure, Sigma-Aldrich, Germany) was used as a photoinitiator with 1 wt % for PEA and 0.35 wt % for PMA. The polymerization reaction was allowed in Schlenk flasks exposing to ultraviolet light (portable UV lamp with light of 390- 410nm) up to the limited conversion of monomers (2 hours). Polymers were then dried to constant weight in a vacuum oven at 60 °C for 12 hours. Both polymers were solubilized in toluene (99.8% pure, Sigma-Aldrich) to concentration of 6% w/v for PEA and 2.5% w/v for PMA. 2 hours sonication in an ultrasonic bath at room temperature was used to make the polymer soluble. Glass slides (76 x 26 mm, Hounisen) were cleaned with sonication in ultrasonic bath for 15 minutes in Acetone, Ethanol, and Milli-Q water respectively, and then dried under nitrogen flow. A thin film of polymer solution was coated on clean slides using spin-coater (Laurell Technologies) with acceleration and velocity of 1000 rpm for 30 seconds. The spin-coated films were degassed in a desiccator for 30 minutes under vacuum and then put in a vacuum oven at 60 °C for 2 hours to remove toluene.

**Fn adsorption to PMA and PEA**

A hydrophobic marker (PAP pen – Sigma-Aldrich) was used to draw a small circle (around 0.5 cm square area) on the spin-coated slides. Fn from human plasma (Sigma-Aldrich, F0895) was dissolved in PBS at concentration of 20 µg $ml^{-1}$ and 100 µl sample was adsorbed on each slide for 1 hour at room temperature.

**Atomic force microscopy for imaging of Fn adsorbed to PMA and PEA**

Experiments were conducted on three replicate samples with JPK Nanowizard IV (JPK, Germany) using HQ: CSC38/No Al (Mikromasch, USA) and TR400PSA (Asylum Research, USA) cantilevers. We used the fluid mode of operation to visualize Fn adsorbed to PEA and PMA without introducing

artifacts from sample drying. The operating environment was controlled in a closed liquid chamber at 21°C with minimal evaporation. The operation parameters were set to optimize resolution with minimum possible damage or artifact from contaminations on the tip. Typically, scans were started with a large scan area of minimum 10 x 10 µm² with a rather low scan resolution of 64 x 64 pixels and a high scan rate > 1 Hz. Once an area of interest was identified, a higher resolution image 256 x 256 or 512 x 512 pixels of a smaller scan are was acquired at lower scan speeds (< 1 Hz). The acquired data was processed using Gwyddion open software (http://gwyddion.net/) for necessary corrections of tilt etc.

**XPS of Fn adsorbed to PEA and PMA**

A100 µl of Fn (20 µg $ml^{-1}$) was adsorbed on a polymer spin-coated 1 × 1 cm glass slides (these slides were cut manually in the chemistry lab workshop) for 1 hour, and samples were then washed three times with Milli-Q water and dried under $N_2$ flow. The chemical composition of the adsorbed layer was analyzed with a Kratos AXIS Ultra DLD instrument equipped with a monochromatic Al K$\alpha$ X-ray source (hν = 1486.6 eV). All spectra were collected in electrostatic mode at a take-off angle of 55° (angle between the sample surface plane and the axis of the analyzer lens). The spectra were collected at new spots on the sample (n=3, 1 replicate) and were charge corrected to the $C_{1s}$ aliphatic carbon binding energy at 285.0 eV, and a linear background was subtracted for all peak areas quantifications. Analyzer pass energy of 160 eV was used for compositional survey scans of $C_{1s}$, $O_{1s}$, $N_{1s}$, $Na_{1s}$, $Si_{2p}$, $Cl_{2p}$, $P_{2p}$, and $K_{2p}$. High-resolution scans of $C_{1s}$ and $N_{1s}$ elements were collected at an analyzer pass energy of 20 eV. Compositions and fits of the high-resolution scans were produced in CasaXPS. The data is presented in a table as an average and standard deviation of the three sample spots.

**FTIR analysis of Fn adsorbed to PEA and PMA**

FTIR measurements were performed on a Bruker Vertex v70 with 128 scans per spectrum and a 7 mm diameter beam spot. The concentration of Fn (20 µg$ml^{-1}$) results in very small IR absorbances of the polymer layers, so therefore, the spectra of stacks of 8 coated CaF2 windows were measured simultaneously. For this, 8 spin coated CaF2 window surfaces with PMA and PEA were incubated for one hour with the 20 µg$ml^{-1}$ Fn solution in PBS prepared in $D_2O$ (d-PBS hereafter), after rinsing the surfaces with d-PBS and placed 4 sets of windows (spaced by 25 µm Teflon spacers that were filled by d-PBS, with the polymer and protein-coated sides submerged in the d-PBS) in a custom-

made IR cell. The incubated sample spectra were background-corrected by subtracting the spectra of the same neat d-PBS loaded windows. Before subtraction, we (i) corrected for small differences in the overall transmission of the protein and background samples (due to e.g. small differences in the amount of scattering of the IR beam, which can become significant with 8 consecutive windows) by subtracting the absorption at 7500 $cm^{-1}$, and (ii) corrected for small differences in the exact water-layer thickness by scaling the spectra using a spectrally isolated absorption band of the D2O (the v1 + v2 combination band of the solvent's OD-bending and stretching mode1 at 3840 $cm^{-1}$) to determine the scaling factor. But there is no reason to assume that the water and polymer layers thicknesses are related. Therefore, the resulting background-corrected amide-I (1600-1700 $cm^{-1}$) PEA+Fn spectrum (Figure 1) still contains a tail of the 1733 $cm^{-1}$ ester peak, which is absent in the resulting PMA+Fn spectrum. This is (i) because there is approximately 6 times more PEA present than PMA (as indicated by a least-square fit that minimized the total intensity of the subtraction of the PMA from the PEA background spectra in the 1700-1760 $cm^{-1}$ region, see supplementary materials Figure S6, S7 and the accompanying supplementary materials text), and (ii) because the Fn incubation results in a slight loss of polymer, which is impossible to compensate for well by subtraction of the polymer spectra, because the 1733 $cm^{-1}$ ester peak shape is affected by the presence of the protein (see figure S6). The broadening of this peak by Fn incubation is probably because the ester groups in contact with the protein are slightly shifted with respect of the more buried ester groups that are not changed by the protein adsorption, resulting in two subpeaks that are slightly offset in frequency. Even though the PMA layer appears to be thinner and/or less dense, it will probably still be composed of many monolayers (as indicated by the XPS measurements), so this difference in thickness is not expected to affect the protein's interfacial behavior.

**Quantification of bacterial attachment under flow**

Ibidi sticky-slide VI 0.4 chambers (Ibidi, Germany) were glued to polymer-coated glass by using an equivalent mixture of silicon (DOWSIL 732 - Dow corning) and UV activating glue (Loctite 3106 Light Cure Adhesive). After flow cell assembly, 50 µl of Fn (20 µg $ml^{-1}$) dissolved in PBS was injected to the channel of a flow cell and allow to adsorb statically for 1 hour at room temperature. The unbound Fn was removed by a flow of PBS (6 ml $hour^{-1}$) using a syringe pump (Harvard Apparatus, USA) for 15 minutes. Bacterial cells were subcultured from an overnight culture and grown for 6 hours at 37°C and 180 rpm, harvested by centrifugation (4000 g for 10 minutes), and

resuspended in PBS to an $OD_{600}$ of 0.1. The cell suspension was flowed through the flow cell chamber at 3 ml $hour^{-1}$ for 2 hours at room temperature. The unbound cells were washed with PBS at 9 ml $hour^{-1}$ for 30 minutes. Attached bacteria were visualized by brightfield microscopy (Zeiss Axiovert A100, 20x objective) and counted. A minimum of 5 images were acquired per replicate, and a minimum of 500 cells were counted per replicate.

The first experiment compared attachment of *S. carnosus* TM300 x pEmbp_5F and *S. carnosus* TM300 x pEmbp_9FG to PEA and PMA surfaces with and without Fn to investigate if the Fn-binding domains of Embp interacted selectively with the fibrillated form of Fn. The second experiment investigated which domain of Fn Embo interacted with. Previous studies had shown that that Embp binds to the F3 $12^{th}$-$14^{th}$ domain of Fn (*11*), however, this experiment was only performed with recombinant fragments of Fn and not the full length protein. We therefore investigated the role of this Fn domain in the attachment of bacteria via Embp. Flow-cell experiments were carried out as described above, comparing attachment via F og FG to fibrillated Fn directly or after blocking for F3 $12^{th}$-$14^{th}$ domain withn IgG antibodies (Anti-Fn, sc-18827, Santa Cruz biotech). As a control, fibrillated Fn was blocked with IgG antibodies specific for another Fn domain (F3 $5^{th}$ domain). The unbound antibodies were removed with PBS (6 ml $hour^{-1}$, 15 minutes) before investigating bacterial attachment as described above.

The final experiment addressing attachment under flow compared the attachment of *S. epidermidis* 1585 Pxyl/tet *embp* and *S. epidermidis* Δ*embp.* The strains were inoculated from single colonies into BHI broth (amended with 5 μg $ml^{-1}$ erythromycin and 200 ng $ml^{-1}$ anhydrotetracycline (ATC) for the Pxyl/tet *embp* strain) and grown overnight at 37°C, 180 rpm, harvested by centrifugation, and resuspended in PBS to $OD_{600}$ = 0.3, transferred to the syringe pump and passed through the flow-cells at either 1 mL $min^{-1}$ or 18 ml $min^{-1}$ flowrate for 1 h followed by a 30 min PBS washing step of 6 ml $min^{-1}$ or 36 ml $min^{-1}$, respectively. Attached cells were imaged by brightfield microscopy and by CLSM after staining with 20x SYBR Green II (Sigma Aldrich).

**Hydrodynamic radius**

*S. epidermidis* 1585 Pxyl/tet *embp* and *S. epidermidis* Δ*embp* were prepared as described above, transferred to cuvettes and analysed by dynamic light scattering (DLS) (Folded Capillary Zeta Cell, malvern US). Measurements of surface charge and cell diameter was carried out using Zetasizer Nano (Malvern Panalytical).

**Single-cell force spectroscopy**

Single-cell force spectroscopy (SCFS) measurements were conducted on Fn adsorbed in its globular conformation to PMA or its fibrillated conformation to PEA. For SCFS measurement, colloidal probes with 10 µm glass beads (SHOCON-BSG-B-5, Applied NanoStructures Inc., USA) were selected and coated by polymerizing a dopamine solution of 4 mg $ml^{-1}$ dopamine hydrochloride (99%, Sigma-Aldrich, H8502) in 10 mM Tris-HCl buffer at pH 8.5, and then calibrated *in situ* for single-cell attachment. *S. carnosus* TM300 expressing 5 F- and 9 FG-repeats were subcultured from overnight cultures and incubated for 6 hours in fresh media, harvested and resuspended in PBS as described above. A 100 µl drop of this solution was placed on a glass slide and incubated for 10 minutes, after which the unadsorbed bacteria were removed by rinsing with PBS. A colloidal probe was immersed and positioned on top of a single cell with the help of inverted optical microscope. The probe was made to contact a single cell for 5 minutes then retracted after the cell attachment. Once a cell was picked up (confirmed by optical microscopy), the substrate was changed to Fn coated surfaces and SCFS was executed. The acquired force-distance plots were processed using the Nanowizard's (JPK, Germany) own processing software. Experiments were conducted on two replicate samples.

**Cloning and purification of F- and FG-repeats**

Genomic DNA was extracted from *S. epidermidis* 1585 WT strain using the Qiagen DNA kit (Qiagen, Hilden, Germany) by following the instructions of the manufacturer. The only exception made in the kit protocol was that cells were lysed with 15 U of lysostaphin, which was added to buffer P1. The nucleotide sequence of one, four, and fifteen repeats of the FG-repeats were amplified from genomic DNA using primers (Table S2) with Phusion High-Fidelity PCR Kit (NEB - E0553S). The PCR products were purified with GenElute PCR Clean-Up Kit (Sigma-Aldrich NA1020). The expression vector pET302/NT-His was digested with EcoR1 restriction enzyme (NEB R0101S) and run on a 1.5 % agarose gel. The digested vector was purified from the gel using the GenElute Gel Extraction Kit (Sigma-Aldrich NA1111). The purified PCR product of each recombinant Embp (rEmbp) was ligated with the digested vector in a ratio of 3:1 using the Gibson assembly ligation matrix mix (NEB E5510S). Each ligation reaction was incubated for 1 hour at 50 °C. The ligated products were transformed into the chemically competent *E. coli* strain (Top10). The colony PCR was performed with REDTaq ReadyMix (Sigma-Aldrich R2523) using the T7 promoter primer as forward and the T7 terminator primer as the reverse. Cells from each selected colony were grown overnight in LB with 100 µg $ml^{-1}$ ampicillin, and a plasmid miniprep was prepared using GeneJET Plasmid Miniprep Kit (Thermo Scientific K0702). Plasmids were sequenced with both T7 promoter

and terminator primers by the Eurofins A/S (Hamburg, Germany). The plasmid of each Embp construct was transformed into an expression system (chemically competent *E. coli*, BL21-DE3). A single colony of the transformants was used to inoculate 2 L of LB with 100 μg $ml^{-1}$ ampicillin until the $OD_{600}$ of 0.6. For the overexpression, cells were induced with 1M IPTG, and incubated for 16 hours on 28 °C in shaking incubator at 180 rpm. Cells were harvested and lysed in binding buffer with sonication (30% amplitude, 15 seconds off, 15 seconds on) for 3 minutes on ice. After centrifugation, the supernatant was filtered with a 0.22 μm syringe filter and run on a Nickel-Nitrilotriacetic Acid (Ni-NTA) column using ÄKTA Purifier-10 purification system. The column was washed with 5 - 8 column volumes, and the fusion proteins Embp was then eluted in fractions using elution buffer. Fractions of each rEmbp were pooled, concentrated with Amicon Ultra centrifugal filter tubes with a cut-off 3 kDa (Millipore Sigma UFC9003). Proteins were further purified with (HiTrap Q FF) column by anion exchange (IEX) chromatography using IEX binding and elution buffer, followed by size exclusion chromatography (SEC) with column (Superdex 200 Increase 10/300 GL) using MES buffer on ÄKTA Purifier-10 purification system. After each column, the elution fractions were run on SDS-PAGE to check the purification quality. Buffers used for rEmbp purification are listed in Table S3.

**Single-molecule force spectroscopy**

Single-molecule force spectroscopy (SMFS) measurements, similar to SCFS, conducted on Fn adsorbed to either PEA and PMA. For the SMFS experiments, the probes were prepared by attaching rEmbp fragments of various lengths with the use of $His_6$-NTA interaction. The procedure was similar to that of Obataya *et al (41)*. In short, silicon probes were cleaned with ozone, and UV light then kept in one to tone isopropyl alcohol and ethanol mixture overnight. Tips were rinsed in deionized water and air-dried, after which they were functionalized with 2% (3-mercaptopropyl) trimethoxysilane in EtOH for 30 minutes. Probes were then exposed to Maleimide-C3-NTA in 50% DMF/100 mM Tris-HCl (pH7.5 ± 0.1) overnight. 10 mM $NiCl_2$ was used to chelate the NTA groups on the tip, which was then dipped in bovine serum albumin (1 mg $ml^{-1}$ in PBS) to passivate the surface. The attachment of 6X His-tagged rEmbp fragments with 1, 4 or 15 repeating units of Fn binding repeats was completed by 1 hour incubation of respective samples at room temperature. After a probe for each repeating unit were prepared, force-distance curves were collected on three replicate samples and processed, as mentioned above.

## ACKNOWLEDGEMENTS

This work was funded by the Carlsberg Foundation, Grant number CF16-0342. Cecilie Siem Bach-Nielsen is gratefully acknowledged for quantification of *S. epidermidis* attachment under high and low flow rates. TWG and SJR thank the Lundbeck Foundation for postdoc fellowships.

## REFERENCES

1. C. R. Arciola, D. Campoccia, L. Montanaro, Implant infections: Adhesion, biofilm formation and immune evasion. *Nature Reviews Microbiology* **16**, 397-409 (2018).
2. W. F. Oliveira *et al.*, Staphylococcus aureus and Staphylococcus epidermidis infections on implants. *Journal of Hospital Infection* **98**, 111-117 (2018).
3. L. de Vor, S. H. M. Rooijakkers, J. A. G. van Strijp, Staphylococci evade the innate immune response by disarming neutrophils and forming biofilms. *FEBS Letters* **594**, 2556-2569 (2020).
4. S. E. Rowe, J. E. Beam, B. P. Conlon, Recalcitrant Staphylococcus aureus Infections: Obstacles and Solutions. *Infection and immunity* **89**, (2021).
5. J. D. Patel, M. Ebert, R. Ward, J. M. Anderson, S. epidermidis biofilm formation: Effects of biomaterial surface chemistry and serum proteins. *Journal of Biomedical Materials Research - Part A* **80**, 742-751 (2007).
6. P. François, P. Vaudaux, P. D. Lew, Role of plasma and extracellular matrix proteins in the physiopathology of foreign body infections. *Annals of Vascular Surgery* **12**, 34-40 (1998).
7. T. J. Foster, Surface Proteins of Staphylococcus epidermidis. *Frontiers in Microbiology* **11**, (2020).
8. H. Rohde *et al.*, Polysaccharide intercellular adhesin or protein factors in biofilm accumulation of Staphylococcus epidermidis and Staphylococcus aureus isolated from prosthetic hip and knee joint infections. *Biomaterials* **28**, 1711-1720 (2007).
9. V. C. Salgueiro, N. L. P. Iorio, M. C. Ferreira, R. C. Chamon, K. R. N. Dos Santos, Methicillin resistance and virulence genes in invasive and nasal Staphylococcus epidermidis isolates from neonates. *BMC Microbiology* **17**, (2017).
10. H. Büttner *et al.*, A giant extracellular matrix binding protein of staphylococcus epidermidis binds surface-immobilized fibronectin via a novel mechanism. *mBio* **11**, 1-9 (2020).
11. M. Christner *et al.*, The giant extracellular matrix-binding protein of Staphylococcus epidermidis mediates biofilm accumulation and attachment to fibronectin. *Molecular Microbiology* **75**, 187-207 (2010).
12. W. Dolores, R. Christian, N. Harald, P. Hildegunde, W. Georg, Cellular and molecular composition of fibrous capsules formed around silicone breast implants with special focus on local immune reactions. *Journal of Autoimmunity* **23**, 81-91 (2004).
13. M. Rocco, O. Aresu, L. Zardi, Conformational state of circulating human plasma fibronectin. *FEBS Letters* **178**, 327-330 (1984).
14. G. Baneyx, L. Baugh, V. Vogel, Coexisting conformations of fibronectin in cell culture imaged using fluorescence resonance energy transfer. *Proceedings of the National Academy of Sciences of the United States of America* **98**, 14464-14468 (2001).
15. C. Zhong *et al.*, Rho-mediated contractility exposes a cryptic site in fibronectin and induces fibronectin matrix assembly. *Journal of Cell Biology* **141**, 539-551 (1998).

16. V. Llopis-Hernández *et al.*, Material-driven fibronectin assembly for high-efficiency presentation of growth factors. *Science Advances* **2**, (2016).
17. P. Rico *et al.*, Substrate-induced assembly of fibronectin into networks: Influence of surface chemistry and effect on osteoblast adhesion. *Tissue Engineering - Part A* **15**, 3271-3281 (2009).
18. M. Salmerón-Sánchez *et al.*, Role of material-driven fibronectin fibrillogenesis in cell differentiation. *Biomaterials* **32**, 2099-2105 (2011).
19. M. K. Bieniek, V. Llopis-Hernandez, K. Douglas, M. Salmeron-Sanchez, C. D. Lorenz, Minor Chemistry Changes Alter Surface Hydration to Control Fibronectin Adsorption and Assembly into Nanofibrils. *Advanced Theory and Simulations* **2**, (2019).
20. N. B. Guerra *et al.*, Subtle variations in polymer chemistry modulate substrate stiffness and fibronectin activity. *Soft Matter* **6**, 4748-4755 (2010).
21. A. Barth, C. Zscherp, What vibrations tell us about proteins. *Quarterly Reviews of Biophysics* **35**, 369-430 (2002).
22. L. Kar *et al.*, 1H NMR-based determination of the three-dimensional structure of the human plasma fibronectin fragment containing inter-chain disulfide bonds. *Journal of Biological Chemistry* **268**, 8580-8589 (1993).
23. J. R. Potts, I. D. Campbell, Structure and function of fibronectin modules. *Matrix Biology* **15**, 313-320 (1996).
24. K. J. Johnson, H. Sage, G. Briscoe, H. P. Erickson, The compact conformation of fibronectin is determined by intramolecular ionic interactions. *Journal of Biological Chemistry* **274**, 15473-15479 (1999).
25. L. M. Maurer, W. Ma, D. F. Mosher, Dynamic structure of plasma fibronectin. *Critical Reviews in Biochemistry and Molecular Biology* **51**, 213-227 (2016).
26. E. Klotzsch *et al.*, Fibronectin forms the most extensible biological fibers displaying switchable force-exposed cryptic binding sites. *Proceedings of the National Academy of Sciences of the United States of America* **106**, 18267-18272 (2009).
27. C. R. Arciola *et al.*, Staphylococcus epidermidis-fibronectin binding and its inhibition by heparin. *Biomaterials* **24**, 3013-3019 (2003).
28. A. Both *et al.*, Distinct clonal lineages and within-host diversification shape invasive staphylococcus epidermidis populations. *PLoS Pathogens* **17**, (2021).
29. A. E. Paharik, A. R. Horswill, in *Virulence Mechanisms of Bacterial Pathogens*. (2016), pp. 529-566.
30. R. J. Williams, B. Henderson, L. J. Sharp, S. P. Nair, Identification of a fibronectin-binding protein from Staphylococcus epidermidis. *Infection and Immunity* **70**, 6805-6810 (2002).
31. I. Maxe, C. Ryden, T. Wadstrom, K. Rubin, Specific attachment of Staphylococcus aureus to immobilized fibronectin. *Infection and Immunity* **54**, 695-704 (1986).
32. M. Paulsson, I. Gouda, O. Larm, Å. Ljungh, Adherence of coagulase-negative staphylococci to heparin and other glycosaminoglycans immobilized on polymer surfaces. *Journal of Biomedical Materials Research* **28**, 311-317 (1994).
33. M. J. Pestrak *et al.*, Investigation of synovial fluid induced Staphylococcus aureus aggregate development and its impact on surface attachment and biofilm formation. *PLoS ONE* **15**, (2020).
34. Y. Tanaka *et al.*, A Helical String of Alternately Connected Three-Helix Bundles for the Cell Wall-Associated Adhesion Protein Ebh from Staphylococcus aureus. *Structure* **16**, 488-496 (2008).
35. D. J. Müller, J. Helenius, D. Alsteens, Y. F. Dufrne, Force probing surfaces of living cells to molecular resolution. *Nature Chemical Biology* **5**, 383-390 (2009).

36. V. Post *et al.*, Comparative genomics study of Staphylococcus epidermidis isolates from orthopedic-device-related infections correlated with patient outcome. *Journal of Clinical Microbiology* **55**, 3089-3103 (2017).
37. J. M. Steckelberg, W. R. Wilson, Risk factors for infective endocarditis. *Infectious Disease Clinics of North America* **7**, 9-19 (1993).
38. W. S. To, K. S. Midwood, Plasma and cellular fibronectin: Distinct and independent functions during tissue repair. *Fibrogenesis and Tissue Repair* **4**, (2011).
39. M. Christner *et al.*, The giant extracellular matrix-binding protein of Staphylococcus epidermidis mediates biofilm accumulation and attachment to fibronectin. *Molecular microbiology* **75**, 187-207 (2010).
40. P. Rico *et al.*, Substrate-induced assembly of fibronectin into networks: influence of surface chemistry and effect on osteoblast adhesion. *Tissue Engineering Part A* **15**, 3271-3281 (2009).
41. I. Obataya, C. Nakamura, S. Han, N. Nakamura, J. Miyake, Direct insertion of proteins into a living cell using an atomic force microscope with a nanoneedle. *Nanobiotechnology* **1**, 347-352 (2005).

## Figure Legends

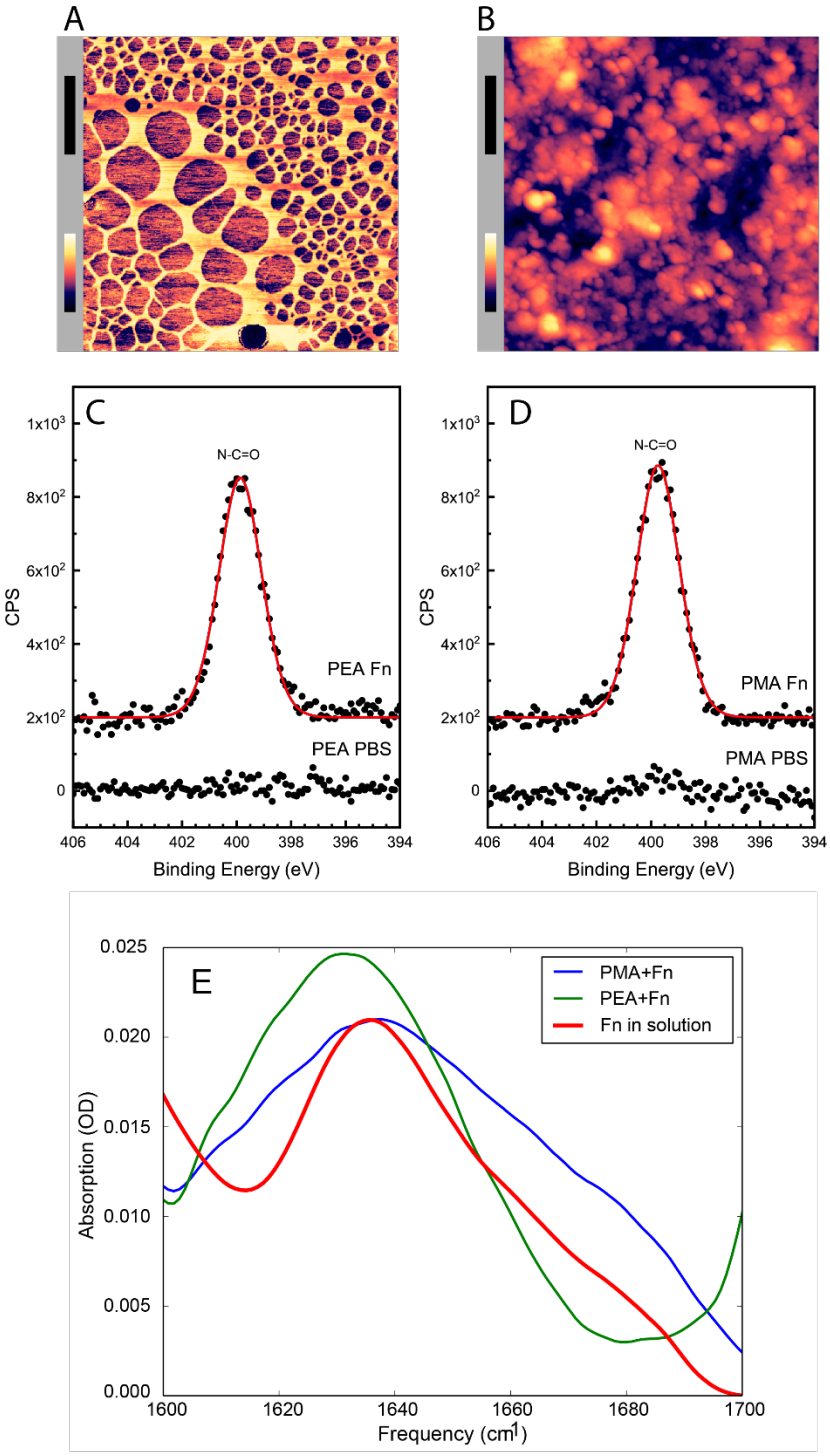


**Figure 1:** The conformation of adsorbed Fn depends on the surface chemistry of a material. AFM imaging shows the structure of adsorbed Fn on A) PMA and C) PEA. The protein remained globular on PMA (black bar is 500 nm, while the (colored) height bar is 0-115 nm), but fibrillated on PEA (black bar is 500 nm, while the (colored) height bar is 0-158 nm). XPS analysis of the samples show similar chemical composition of Fn adsorbed to B) PMA and D) PEA, indicating that two polymer surfaces have the same amount of adsorbed Fn.

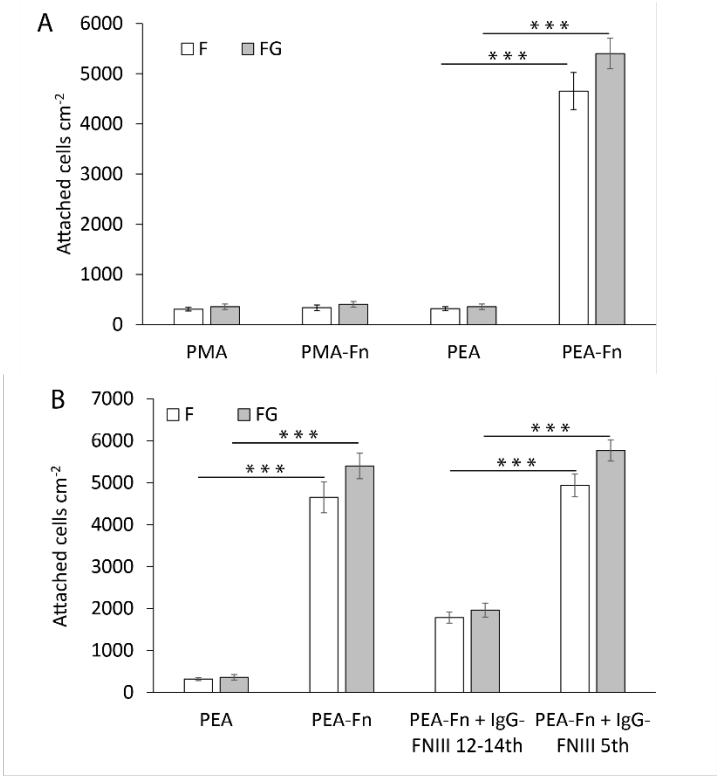


**Figure 2:** Embp-mediated bacterial attachment to globular and fibrillated Fn adsorbed to PEA or PMA-coated surfaces. A) *S. carnosus* TM300 expressing either F- or FG-repeats were passed through flow cells for 2 hours before enumeration of attached cells by microscopy. Adsorbed Fn only promoted attachment on PEA-coated surfaces where Fn fibrillated. B) Identification of the Fn domain involved in bacterial attachment. The F3 $12^{th}$-$14^{th}$ repeats were blocked with a specific antibody prior to exposing bacteria to the surfaces. Blocking of the F3 $5^{th}$ domain was included as a control for non-specific blocking of Fn by the antibodies. Values are averages from three independent experiments (error bars = S.D.). The two-tailed P-value from t test is $< 0.0001$.

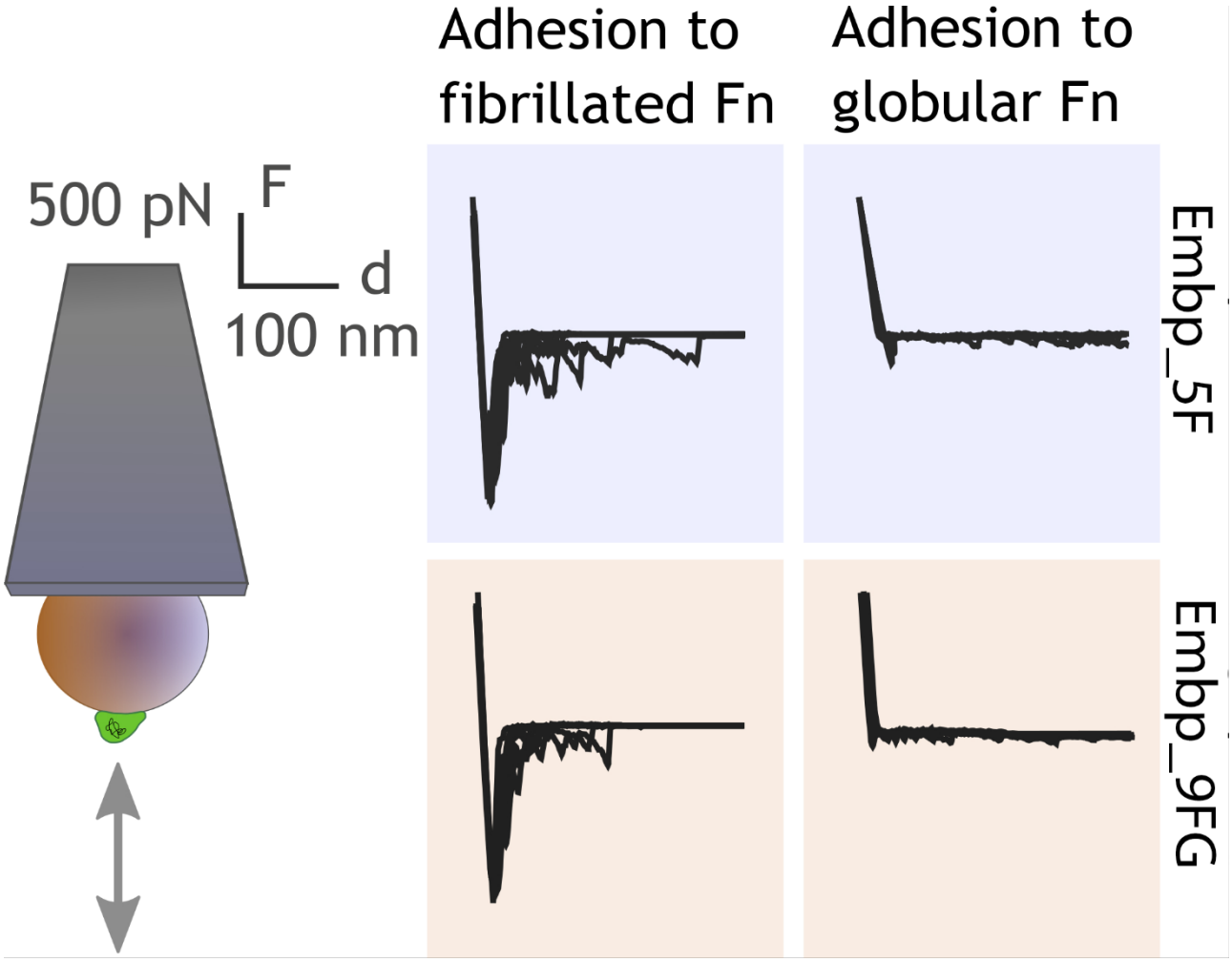


**Figure 3:** Single cell force spectroscopy shows that both the F- and FG-repeats adheres strongly to fibrillated Fn on PEA compared to the globular Fn on PMA. Single *S. carnosus* TM300 expressing either F- or FG-repeats on the cell surface were immobilized on a colloidal AFM cantilever, and force-distance curves were measured from interaction with fibrillated Fn on PEA or globular Fn on PMA.

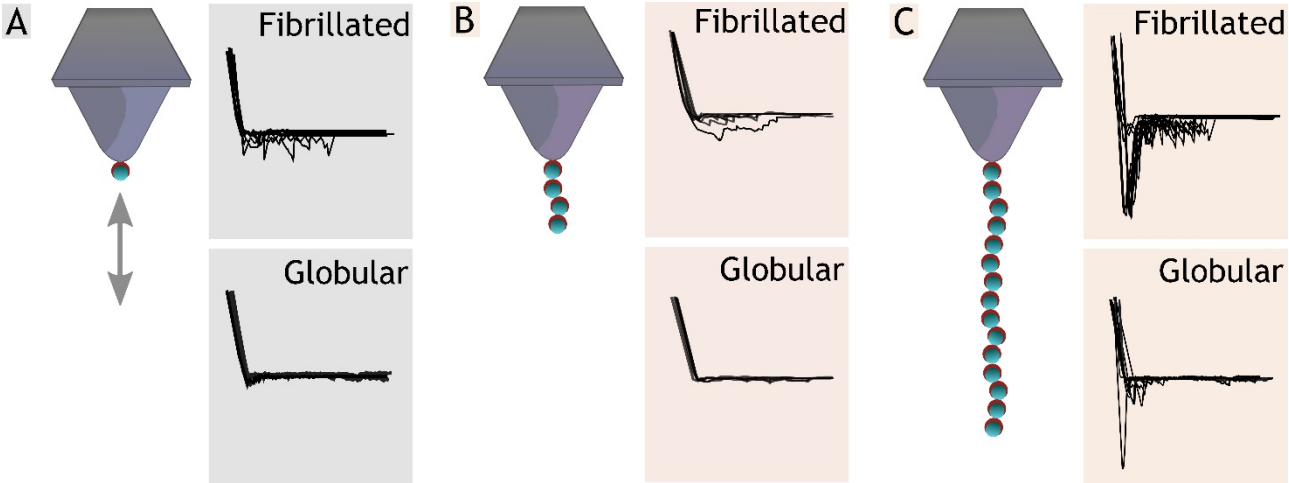


**Figure 4:** Single molecule force spectroscopy shows that rEmbp with 15 FG-repeats have multiple interactions with fibrillated Fn, while interactions forces with a single and four FG-repeats are below the detection limit. rEmbp were tethered to a chemically modified silicon probe trough 6X His-NTA interaction. Force distance curves were measured of these repeats towards fibrillated Fn on PEA and globular Fn on PMA.

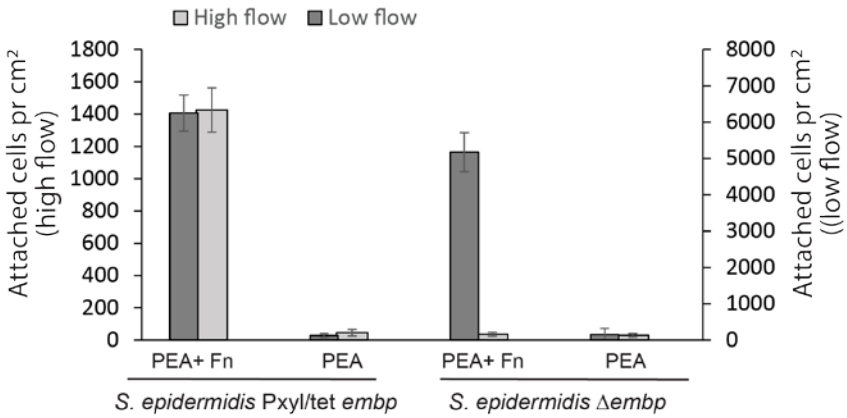


**Figure 5.** Attachment of *S. epidermidis* lacking Embp or over-expressing Embp. Cells only attached to surfaces with adsorbed, fibrillated Fn. At low flow, Embp had little impact on attachment. But at high flow, Embp was a prerequisite for attachment.

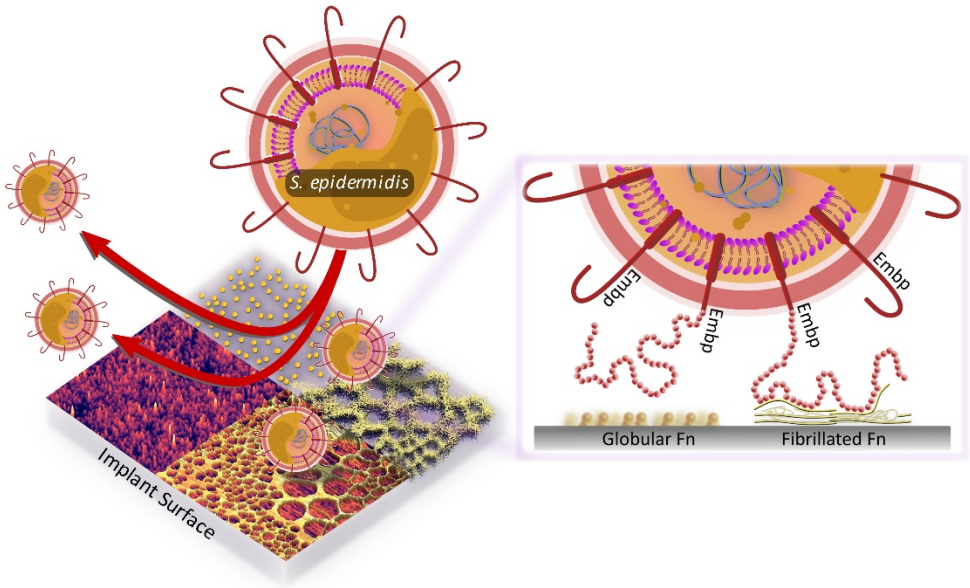


**Graphical abstract:** Fibronectin exists in two different conformations in the body. It circulates in the bodily fluids in globular conformation, however, it become fibrillated once adsorbed to an implant surface. *S. epidermidis* possess a giant 1 MDa receptor known as Embp bind specifically to fibrillated Fn but not to the globular Fn.